

The effect of post-Newtonian spin precessions on the evolution of exomoons' obliquity

Lorenzo Iorio¹

Ministero dell'Istruzione, dell'Università e della Ricerca (M.I.U.R.)

Viale Unità di Italia 68, I-70125, Bari (BA), Italy

`lorenzo.iorio@libero.it`

Received _____; accepted _____

Abstract

Putative natural massive satellites (exomoons) has gained increasing attention, where they orbit Jupiter-like planets within the habitable zone of their host main sequence star. An exomoon is expected to move within the equatorial plane of its host planet, with its spin \mathbf{S} aligned with its orbital angular momentum \mathbf{h} which, in turn, is parallel to the planetary spin \mathbf{J} . If, in particular, the common tilt of such angular momenta to the satellite-planet ecliptic plane, assumed fixed, has certain values, the latitudinal irradiation experienced on the exomoon from the star may allow it to sustain life as we know it, at least for certain orbital configurations. An Earth-analog (similar in mass and obliquity) is considered, which orbits within $5 - 10$ planetary radii R from its Jupiter-like host planet. The de Sitter and Lense–Thirring spin precessions due to the general relativistic post-Newtonian (pN) field of the host planet have an impact on an exomoon’s habitability. Here, I show it by identifying long-term variations in the satellite’s obliquity ε , where variations can be $\lesssim 10^\circ - 100^\circ$, depending on the initial spin-orbit configuration, with a timescale of $\simeq 0.1 - 1$ million years.

Subject headings: Planets and satellites: general – Astrobiology – Gravitation – Celestial mechanics – Methods: analytical – Methods: numerical

1. Introduction

In investigating the possibility that alien worlds, extrasolar planets (Seager 2011; Lissauer 2012; Deeg & Belmonte 2018; Perryman 2018) and related environments, may host and sustain known (and unknown) forms of life and, possibly, civilizations (Kaltenegger 2017; Schulze-Makuch & Bains 2018; Schwieterman et al. 2018; Irwin & Schulze-Makuch 2020), it is of crucial importance to assess the physical conditions posing tight constraints. In this framework, I will look at a novel scenario, where Einstein’s General Theory of Relativity (GTR; Debono & Smoot 2016; Misner, Thorne & Wheeler 2017) may have a direct, macroscopic impact on life and its long-term sustainability.

Natural satellites of Jupiter-like gas giants, or exomoons (Barnes & O’Brien 2002; Domingos, Winter & Yokoyama 2006; Heller et al. 2014; Schneider, Lainey & Cabrera 2015), could be habitable if the host planet orbits within the habitable zone of its main sequence star (Williams, Kasting & Wade 1997; Kaltenegger 2010; Heller, R. 2012; Forgan & Kipping 2013; Heller & Barnes 2013; Hinkel & Kane 2013; Heller et al. 2014; Dobos, Heller & Turner 2017; Zollinger, Armstrong & Heller 2017; Hill et al. 2018; Forgan, D. 2019; Martínez-Rodríguez et al. 2019; Lingam & Loeb 2020; Tjoa, Mueller & van der Tak 2020). Exomoons’ mass m should be $0.25 m_{\oplus} \lesssim m \lesssim 2 m_{\oplus}$ to sustain life over a billion-year timescale (Heller & Barnes 2013). According to Sasaki, Stewart & Ida (2010), their actual formation around extrasolar giant planets is possible. Still unconfirmed exomoons candidates exist (Fox & Wiegert 2021; Teachey & Kipping 2018). The project Hunt for Exomoons with Kepler (HEK) was the most important effort aimed to detect exomoons to date (Kipping et al. 2012, 2013b,a; Teachey, Kipping & Schmitt 2018). Searches for exomoons started in 2009 (Kipping 2009a,b; Kipping, Fossey & Campanella 2009), after theoretical investigations about such a possibility (Sartoretti & Schneider 1999; Cabrera & Schneider 2007). Techniques to be used in exomoons’ detection are transit timing variations (TTVs), transit duration variations (TDVs), and apparent planetary transit radius variations (TRVs) (Rodenbeck, Heller & Gizon 2020); according to Rodenbeck, Heller & Gizon (2020), TRVs could be a more promising means to identify exomoons in large exoplanet surveys.

Such exomoons could be tidally locked to their parent planet but not to the host star, and moving in the planetary equatorial plane due to tidal evolution (Porter & Grundy 2011; Heller & Barnes 2013). Moreover, the satellite’s spin S should be parallel to the orbital angular momentum h of the planetocentric motion (Heller & Barnes 2013). Thus, the exomoon should have the same obliquity with respect to the circumstellar orbit as the planetary spin J (Heller & Barnes 2013), so that it could experience seasons if the equator of the host planet is tilted against the ecliptic plane (Heller & Barnes 2013). Such a scenario is plausible because previous studies have shown that exomoons can maintain significant obliquities on large timescales (Heller, Leconte & Barnes 2011; Heller & Barnes 2013).

One of the key parameters for the long-term habitability of an astronomical major body is the axial tilt ε , or obliquity, of its spin to its orbital plane, and its long-term stability over the æons. In the case of a star-planet scenario, the planetary axial tilt ε to

the ecliptic plane is crucial for the latitude-dependent insolation received from the host star (Laskar, Joutel & Robutel 1993; Williams & Kasting 1997; Laskar et al. 2004; Armstrong et al. 2014; Linsenmeier, Pascale & Lucarini 2015; Quarles et al. 2019; Kilic, Raible & Stocker 2017; Shan & Li 2018; Quarles, Li & Lissauer 2019). Indeed, variations in obliquity, meant as difference between its extreme values, drive changes in planetary climate. If the obliquity variations are rapid and/or large, the resulting climate shifts can be commensurately severe (Armstrong, Leovy & Quinn 2004). As far as the Earth is concerned, its obliquity changes slowly with time from $\approx 22^\circ.1$ to $24^\circ.5$, undergoing an oscillation cycle with amplitude $\lesssim 2^\circ.4$ in about 41,000 yr (Quarles, Li & Lissauer 2019). The value of the Earth’s obliquity impacts the seasonal cycles and its long-term variation affects the terrestrial climate (Milankovitch 1941), as deduced from geologic records (Kerr 1987; Mitrovica & Forte 1995; Pais et al. 1999). For an exomoon, tidal heating, reflected light by the planet, and the planet’s own infrared irradiation affects the total energy budget in addition to the direct stellar radiation (Heller & Barnes 2013). Thus, it is arguable that the long-term changes of the obliquity relative to the circumplanetary orbital plane will also affect the climate of the exomoon.

The purpose of this paper is to show that GTR may directly affects the habitability of an exomoon through the gravitoelectric de Sitter (de Sitter 1916; Schouten 1918; Fokker 1920) and gravitomagnetic Lense-Thirring¹ (Pugh 1959; Schiff 1960) precessions of its spin S relative to the ecliptic. They are induced by the post-Newtonian (pN) static and stationary components of the gravitational field of its parent planet (Ohanian & Ruffini 2013; Poisson & Will 2014). To the benefit of a reader not acquainted with GTR, the pN expansion is one of the most successful and famous approximation schemes that have been developed in the past years for solving the fully nonlinear Einstein’s equations to describe motions of arbitrary shaped, massive bodies (Asada & Futamase 1997; Blanchet 2003; Will 2018). Furthermore, the terms “gravitoelectric” and “gravitomagnetic” have nothing to do with electric charges and currents, referring, instead, to the formal resemblance of the linearized Einstein field equations of GTR, valid in the slow-motion and weak-field approximation, with the linear Maxwellian equations of electromagnetism (Thorne, MacDonald & Price 1986; Mashhoon 2001; Rindler 2001). Both such effects were successfully measured some years ago in the dedicated spaceborne experiment Gravity Probe B (GP-B) with four artificial gyroscopes orbiting in the field of the Earth (Everitt et al. 2011, 2015). The de Sitter precession was detected also by monitoring the heliocentric motion of the Earth-Moon system (Williams, Newhall & Dickey 1996; Williams & Folkner 2009; Hofmann & Müller 2018), thought of as a giant natural gyroscope, with the Lunar Laser Ranging (LLR) technique (Dickey et al. 1994), and in some binary pulsar systems as well (Breton et al. 2008; Kramer 2012).

For simplicity, I will adopt the scenario by Heller & Barnes (2013) consisting of a main

¹Such a denomination for the pN spin precession induced by the primary’s angular momentum has become of common use, despite it was discovered by Pugh and Schiff in the sixties of the twentieth century.

sequence star orbited at 1 astronomical unit (au) by a gravitationally bound restricted two-body system made of a Jupiter-like planet and an Earth-mass exomoon which, under not too restrictive assumptions, may harbour life. In fact, exomoons may exist also in the habitable zone of M dwarfs (Martínez-Rodríguez et al. 2019; Trifonov et al. 2020), but, in this case, the analysis would be more involved because of the direct dynamical and tidal effects of the star itself. It will be shown that, for the range of plausible distances allowed to the exomoon in order to be habitable (Heller & Barnes 2013), its obliquity relative to the ecliptic may undergo pN variations of tens and even hundreds of degrees depending on the spin-orbit configuration over $\simeq 0.1 - 1$ Myr. I will neglect the presence of other planets in the system, so that the ecliptic plane, assumed as reference coordinate $\{x, y\}$ plane, stays fixed. The orbit of the exomoon around its host planet will be circular, with a size of 5 to 10 planetary radii R (Heller & Barnes 2013). As far as the exomoon’s primary is concerned, I will, first, assume the physical parameters of Jupiter. Then, I will look also at other more massive, larger and more rapidly spinning prototypical gaseous giant planet having the properties of one of those recently characterized in Bryan et al. (2020). It should be stressed that, by placing the planet-satellite system at 1 au from the star, the GTR spin precessions considered here are not due to the pN components of the star’s gravitational field; moreover, it can be reasonably assumed that the ecliptic plane is not perturbed too much by the post-Keplerian (pK), Newtonian or pN, components of the stellar field which are able to induce long-term orbital variations. Instead, they are induced by the planet’s pN field itself; thus, the sources of the de Sitter and Lense-Thirring precessions of the exomoon’s spin are the mass M and the spin angular momentum \mathbf{J} of the Jupiter-type gas giant, respectively (Ohanian & Ruffini 2013; Poisson & Will 2014). As such, they are present independently of any peculiar characteristic of the exomoon itself like, e.g., its quadrupole mass moment, Love number, etc., which may induce their own long-term changes in the obliquity of its spin.

The paper is organized as follows. In Section 2, analytical expressions for the pN rates of change of the satellite’s spin axis with respect to a fixed reference plane are derived, and some qualitative features of their solution for ε are discussed. They are numerically integrated for the case of a Jupiter-like host planet in Section 3, and for a different gaseous giant body in Section 4 by suitably varying the system’s parameter space in both cases. Section 5 summarizes my findings and offer my conclusions.

2. The de Sitter and Lense-Thirring precessions of the spin’s obliquity to the ecliptic plane

2.1. The analytical equations of the pN precessions

Let me assume a coordinate system whose reference $\{x, y\}$ plane coincides with the ecliptic plane of the planet-satellite binary. As parameterization of the satellite’s spin axis $\hat{\mathbf{S}}$, I adopt

$$\hat{S}_x = \sin \varepsilon \cos \alpha, \quad (1)$$

$$\hat{S}_y = \sin \varepsilon \sin \alpha, \quad (2)$$

$$\hat{S}_z = \cos \varepsilon, \quad (3)$$

so that α is the spin's azimuthal angle and ε is its obliquity to the ecliptic: $\varepsilon = 0^\circ$ means that the spin is perpendicular to it. From Equations (1)-(3), it can be straightforwardly obtained

$$\frac{d\varepsilon}{dt} = -\csc \varepsilon \frac{d\hat{S}_z}{dt}, \quad (4)$$

$$\frac{d\alpha}{dt} = \csc \varepsilon \left(\cos \alpha \frac{d\hat{S}_y}{dt} - \sin \alpha \frac{d\hat{S}_x}{dt} \right). \quad (5)$$

To the pN order, the general relativistic rates of change of ε , α , averaged over one orbital revolution of the satellite about its parent planet, can be inferred from the sum of the pN de Sitter and Lense-Thirring averaged precessions of \hat{S}

$$\frac{d\hat{S}}{dt} = (\mathbf{\Omega}_{\text{dS}} + \mathbf{\Omega}_{\text{LT}}) \times \hat{S}, \quad (6)$$

where (Barker & O'Connell 1975; Poisson & Will 2014)

$$\mathbf{\Omega}_{\text{dS}} = \frac{3 n_b \mu}{2 c^2 a (1 - e^2)} \hat{\mathbf{h}}, \quad (7)$$

$$\mathbf{\Omega}_{\text{LT}} = \frac{G J}{2 c^2 a^3 (1 - e^2)^{3/2}} [\hat{\mathbf{J}} - 3 (\hat{\mathbf{J}} \cdot \hat{\mathbf{h}}) \hat{\mathbf{h}}]. \quad (8)$$

In Equations (7)-(8), c is the speed of light in vacuum, G is the Newtonian gravitational constant, $\mu \doteq GM$ is the planet's gravitational parameter, a , e are the semimajor axis and the eccentricity, respectively, of the satellite's planetocentric orbit, $n_b = \sqrt{\mu/a^3}$ is the Keplerian mean motion, $\hat{\mathbf{h}} = \{\sin I \sin \Omega, -\sin I \cos \Omega, \cos I\}$ is the unit vector of the orbital angular momentum, I is the inclination of the satellite's orbital plane to the ecliptic, and Ω is its longitude of the ascending node. By parameterizing the planet's spin axis $\hat{\mathbf{J}}$ as

$$\hat{J}_x = \sin \eta \cos \varphi, \quad (9)$$

$$\hat{J}_y = \sin \eta \sin \varphi, \quad (10)$$

$$\hat{J}_z = \cos \eta, \quad (11)$$

where η , φ are its obliquity and azimuthal angle, respectively, from Equations (1)-(11), one finally gets

$$\begin{aligned} \frac{d\varepsilon}{dt} = & -\frac{3 n_b \mu \sin I \cos \zeta}{2 c^2 a (1 - e^2)} + \\ & + \frac{G J}{4 c^2 a^3 (1 - e^2)^{3/2}} \left[\sin \eta (\sin \xi - 3 \sin \chi) + 3 \cos \zeta (\cos \eta \sin 2I + 2 \cos^2 I \sin \eta \sin \psi) \right], \end{aligned} \quad (12)$$

$$\begin{aligned} \frac{d\alpha}{dt} = & \frac{3 n_b \mu (\cos I + \cot \varepsilon \sin I \sin \zeta)}{2 c^2 a (1 - e^2)} - \\ & - \frac{G J}{8 c^2 a^3 (1 - e^2)^{3/2}} \left\{ \cos \eta (2 + 6 \cos^2 I - 6 \sin^2 I + 6 \cot \varepsilon \sin 2I \sin \zeta) + \right. \\ & \left. + \sin \eta [(\cos \xi + 3 \cos \chi) \cot \varepsilon - 6 (\sin 2I - \cos 2I \cot \varepsilon \sin \zeta) \sin \psi] \right\}, \end{aligned} \quad (13)$$

with

$$\zeta \doteq \alpha - \Omega, \quad (14)$$

$$\xi \doteq \alpha - \varphi, \quad (15)$$

$$\psi \doteq \varphi - \Omega, \quad (16)$$

$$\chi \doteq \varphi + \alpha - 2\Omega. \quad (17)$$

Equations (14)-(17) are relative nodes. In terms of the parameterization of Equations (1)-(3) and Equations (9)-(11), the azimuthal angle Ξ of $\hat{\mathbf{h}}$ is related to Ω by

$$\Omega = 90^\circ + \Xi. \quad (18)$$

If $\hat{\mathbf{S}}$, $\hat{\mathbf{h}}$, $\hat{\mathbf{J}}$ are aligned with each other, i.e. for $\varepsilon = I = \eta$ and $\alpha = \Xi = \varphi$, it is

$$\zeta = -90^\circ, \quad (19)$$

$$\xi = 0, \quad (20)$$

$$\psi = -90^\circ, \quad (21)$$

$$\chi = -180^\circ, \quad (22)$$

so that Equations (12)-(13) vanish.

In obtaining the averaged rates of Equations (12)-(13), it was assumed that ε , α stay essentially constant over one satellite's orbital period, and that I , Ω are fixed, i.e. a Keplerian ellipse was used as unperturbed, reference trajectory in the averaging procedure. Such an assumption is justified by the fact that the exomoon's orbital period amounts just to a few days, while the characteristic timescale of its spin precession is of the order of $\approx 0.1 - 1\text{Myr}$ (see Sections 3 to 4). In fact, a long-term modulation is introduced in Equations (12)-(13) by I , Ω since, actually, they do vary because of a number of classical and general relativistic pK precessions the most important of which are the classical ones due to the planetary oblateness J_2 and the pN Lense-Thirring effect caused by the planet's spin \mathbf{J} . Their characteristic timescales are much longer than the orbital period by several orders of magnitude since they can be calculated perturbatively by averaging out their Gauss equations over one orbital revolution; the quadrupolar and the Lense-Thirring accelerations (Brumberg 1991; Soffel & Han 2019) are, indeed, orders of magnitude smaller than the Newtonian monopole one. By using Equations (1)-(3) and Equations (9)-(11), the classical and relativistic pK averaged rates of change of I , Ω for an arbitrary orientation of the primary's spin axis (Barker & O'Connell 1975; Damour & Schafer 1988; Damour & Taylor 1992; Will 2008; Iorio 2017)

$$\frac{dI}{dt} = -\frac{3 n_b R^2 J_2 (\hat{\mathbf{J}} \cdot \hat{\mathbf{l}}) (\hat{\mathbf{J}} \cdot \hat{\mathbf{h}})}{2 a^2 (1 - e^2)^2} + \frac{2 G J (\hat{\mathbf{J}} \cdot \hat{\mathbf{l}})}{c^2 a^3 (1 - e^2)^{3/2}}, \quad (23)$$

$$\frac{d\Omega}{dt} = -\frac{3 n_b R^2 J_2 \csc I (\hat{\mathbf{J}} \cdot \hat{\mathbf{m}}) (\hat{\mathbf{J}} \cdot \hat{\mathbf{h}})}{2 a^2 (1 - e^2)^2} + \frac{2 G J \csc I (\hat{\mathbf{J}} \cdot \hat{\mathbf{m}})}{c^2 a^3 (1 - e^2)^{3/2}}, \quad (24)$$

where $\hat{\mathbf{l}} = \{\cos \Omega, \sin \Omega, 0\}$ is the unit vector directed along the line of the nodes, which is the intersection of the satellite's orbital plane with the ecliptic, toward the longitude of the ascending node, and $\hat{\mathbf{m}} = \{-\cos I \sin \Omega, \cos I \cos \Omega, \sin I\}$ is the unit vector directed in the orbital plane such that $\hat{\mathbf{l}} \times \hat{\mathbf{m}} = \hat{\mathbf{h}}$, can be cast into the form

$$\begin{aligned} \frac{dI}{dt} = & \frac{3 n_b R^2 J_2 \cos \psi \sin \eta (-\cos I \cos \eta + \sin I \sin \eta \sin \psi)}{2 a^2 (1 - e^2)^2} + \\ & + \frac{2 G J \sin \eta \cos \psi}{c^2 a^3 (1 - e^2)^{3/2}}, \end{aligned} \quad (25)$$

$$\frac{d\Omega}{dt} = -\frac{3 n_b R^2 J_2 \sin I (\cos \eta + \cot I \sin \eta \sin \psi) (\cot I \cos \eta - \sin \eta \sin \psi)}{2 a^2 (1 - e^2)^2} +$$

$$+ \frac{2 G J (\cos \eta + \cot I \sin \eta \sin \psi)}{c^2 a^3 (1 - e^2)^{3/2}}. \quad (26)$$

Equations (23)-(24) can be expressed in compact, vectorial form as (Barker & O’Connell 1975)

$$\frac{d\hat{\mathbf{h}}}{dt} = (2 \boldsymbol{\Omega}_{\text{dS}} + 4 \boldsymbol{\Omega}_{\text{LT}} + \boldsymbol{\Omega}_{J_2}) \times \hat{\mathbf{h}}, \quad (27)$$

where $\boldsymbol{\Omega}_{\text{dS}}$, $\boldsymbol{\Omega}_{\text{LT}}$ are given by Equations (7)-(8), respectively, and (Barker & O’Connell 1975)

$$\boldsymbol{\Omega}_{J_2} = -\frac{3 n_b J_2 R^2}{4 a^2 (1 - e^2)^2} \left\{ 2 (\hat{\mathbf{J}} \cdot \hat{\mathbf{h}}) \hat{\mathbf{J}} + \left[1 - 5 (\hat{\mathbf{J}} \cdot \hat{\mathbf{h}})^2 \right] \hat{\mathbf{h}} \right\}. \quad (28)$$

Note that Equation (27) strictly holds in the test particle limit of the full two-body expressions by Barker & O’Connell (1975). Equations (25)-(26) vanish for Equations (19)-(22). Thus, also the orbital angular momentum stay fixed in space if $\hat{\mathbf{S}}$, $\hat{\mathbf{h}}$, $\hat{\mathbf{J}}$ are aligned, as it can straightforwardly be inferred from Equations (7)-(8) and Equation (27).

Equations (12)-(13) and Equations (25)-(26) represent a system of nonlinear first order differential equations for the four unknowns ε , α , I , Ω to be simultaneously integrated; the angles η , φ of $\hat{\mathbf{J}}$ are assumed to be constant.

2.2. Some qualitative features of the pN obliquity precessions

In order to grasp some essential features of the numerically integrated time series displayed in Sections 3 to 4, I will make some considerations about Equations (12)-(13) and Equations (25)-(26).

Let me define

$$\nu_{\text{dS}} \doteq \frac{3 n_b \mu}{2 c^2 a (1 - e^2)}, \quad (29)$$

$$\nu_{\text{LT}} \doteq \frac{G J}{c^2 a^3 (1 - e^2)^{3/2}}, \quad (30)$$

$$\nu_{J_2} \doteq \frac{3 n_b J_2 R^2}{2 a^2 (1 - e^2)^2}, \quad (31)$$

so that

$$\Lambda_{\text{dS}}^{\text{LT}} \doteq \frac{\nu_{\text{LT}}}{\nu_{\text{dS}}} = \frac{2 J}{3 \sqrt{M^3 G a (1 - e^2)}}, \quad (32)$$

$$\Delta_{J_2}^{\text{LT}} \doteq \frac{2 \nu_{\text{LT}}}{\nu_{J_2}} = \frac{4 G J \sqrt{1 - e^2}}{3 c^2 a n_{\text{b}} R^2 J_2}, \quad (33)$$

$$\Gamma_{\text{dS}}^{J_2} \doteq \frac{\nu_{J_2}}{\nu_{\text{dS}}} = \frac{c^2 J_2 R^2}{\mu a (1 - e^2)}. \quad (34)$$

For a circular orbit at $5 R \leq a \leq 10 R$ from a Jupiter-like host planet, it is

$$\Lambda_{\text{dS}}^{\text{LT}} \simeq 0.03, \quad (35)$$

$$\Delta_{J_2}^{\text{LT}} \simeq 5 \times 10^{-7}, \quad (36)$$

$$\Gamma_{\text{dS}}^{J_2} \simeq 10^5. \quad (37)$$

It implies that, in the considered scenario, the Lense-Thirring spin and orbital precessions can generally be neglected with respect to the de Sitter and quadrupolar ones, respectively, apart from some particular spin and orbital configurations. Also in such an approximated case, it is not possible to obtain analytical solutions from the simultaneous integration of Equations (12)-(13) and Equations (25)-(26) for an arbitrary spin-orbit configuration. Nonetheless, some qualitative features, which will allow to understand certain aspects of the numerically integrated time series in Section 4 with respect to those in Section 3, can still be inferred. Equations (12)-(13) can be combined obtaining

$$\frac{d\varepsilon}{d\alpha} \simeq - \frac{\tan I \cos \zeta}{1 + \tan I \cot \varepsilon \sin \zeta}, \quad (38)$$

where

$$\frac{d\alpha}{dt} \simeq \nu_{\text{dS}} \cos I (1 + \tan I \cot \varepsilon \sin \zeta). \quad (39)$$

Equation (38) implies that, whether I and Ω vary or not, the amplitude of $\varepsilon(\alpha)$ is independent of either the exomoon's distance from the planet and the physical parameters of the latter up to the order of $O(\Lambda_{\text{dS}}^{\text{LT}})$, depending only on the initial spin-orbit configuration. Furthermore, Equation (39) tells that, however complicated the dependence of α on t may be, the characteristic time scale of the resulting time series of $\varepsilon(t)$, which is generally not a simple harmonic function, is determined by Equation (29). Such features can be explicitly inferred in some particular cases like, e.g., in a purely de Sitter scenario. According to Equations (25)-(26), it is $I = I_0$, $\Omega = \Omega_0$ for $J_2 = J = 0$. Then, by analytically solving Equation (6) with Equation (7) only, it is possible to

obtain

$$\begin{aligned} \hat{S}_z(t) = \cos \varepsilon(t) = \cos^2 I_0 \cos \varepsilon_0 + \cos \varepsilon_0 \cos(\nu_{\text{ds}} t) \sin^2 I_0 + \sin \varepsilon_0 [\cos \zeta_0 \sin I_0 \sin(\nu_{\text{ds}} t) - \\ - \sin 2I_0 \sin^2\left(\frac{\nu_{\text{ds}}}{2} t\right) \sin \zeta_0], \end{aligned} \quad (40)$$

where $\zeta_0 \doteq \alpha_0 - \Omega_0$.

3. The case of a Jupiter-like parent planet

I numerically integrated Equations (12)-(13) along with Equations (25)-(26) over 1 – 50 Myr for a fictitious exomoon circling a planet with the same physical parameters of Jupiter along a circular orbit at a few radii from it, as per Heller & Barnes (2013). About the initial conditions, I, first, looked at different mutual orientations of $\hat{\mathbf{S}}, \hat{\mathbf{h}}, \hat{\mathbf{J}}$ for a fixed satellite’s planetocentric distance $a = 5 R$; the time span common to such integrations, shown in Figures 1 to 4, is 1 Myr. Then, in Figure 5, I varied a from $5 R$ to $10 R$ for a given spin-orbit configuration, and extended the integration over 50 Myr.

The case of a close, although not perfect, mutual alignment of $\hat{\mathbf{h}}, \hat{\mathbf{J}}, \hat{\mathbf{S}}$ is shown in Figure 1, based on the initial conditions of Table 1. I allowed for offsets of a few degrees among the spherical angles of the three angular momenta with respect to, say, $\{\theta\} = 23^\circ.44$, $\{\phi\} = 150^\circ$, where $\{\theta\} \doteq \varepsilon_0, I_0, \eta$ and $\{\phi\} \doteq \alpha_0, \Xi_0, \varphi$. The resulting ranges $\varepsilon_{\text{max}} - \varepsilon_{\text{min}}$ of the time series of Figure 1 are still potentially significant for life since their sizes are of the order of $\simeq 3^\circ - 17^\circ$ over characteristic timescales as short as 0.7 Myr, as resumed in Table 1.

Table 1: Initial conditions used in Figure 1. Each row corresponds to the plotted times series with the same roman numeral in the legend of Figure 1. Recall that the azimuthal angle of $\hat{\mathbf{h}}$ is $\Xi = \Omega - 90^\circ$. T is the characteristic timescale, and $\varepsilon_{\text{max}} - \varepsilon_{\text{min}}$ is the full range of variation of the exomoon’s obliquity to the ecliptic.

	$a (R)$	e	$I_0 (^\circ)$	$\Omega_0 (^\circ)$	$\eta (^\circ)$	$\varphi (^\circ)$	$\varepsilon_0 (^\circ)$	$\alpha_0 (^\circ)$	$T (\text{Myr})$	$\varepsilon_{\text{max}} - \varepsilon_{\text{min}} (^\circ)$
I)	5	0.0	25 $^\circ$.44	233	29 $^\circ$.44	147	21 $^\circ$.44	149	0.7	16
II)	5	0.0	28 $^\circ$.44	243	18 $^\circ$.44	146	25	151	0.7	13
III)	5	0.0	22 $^\circ$.44	248	24 $^\circ$.44	148	20.50	153	0.7	10
IV)	5	0.0	21 $^\circ$.7	242	27 $^\circ$.44	156	19	150	0.7	17
V)	5	0.0	20 $^\circ$.44	240	22 $^\circ$.44	153	23 $^\circ$.44	154	0.7	3
VI)	5	0.0	19 $^\circ$.44	238	20 $^\circ$.44	152	24 $^\circ$.20	147	0.7	9

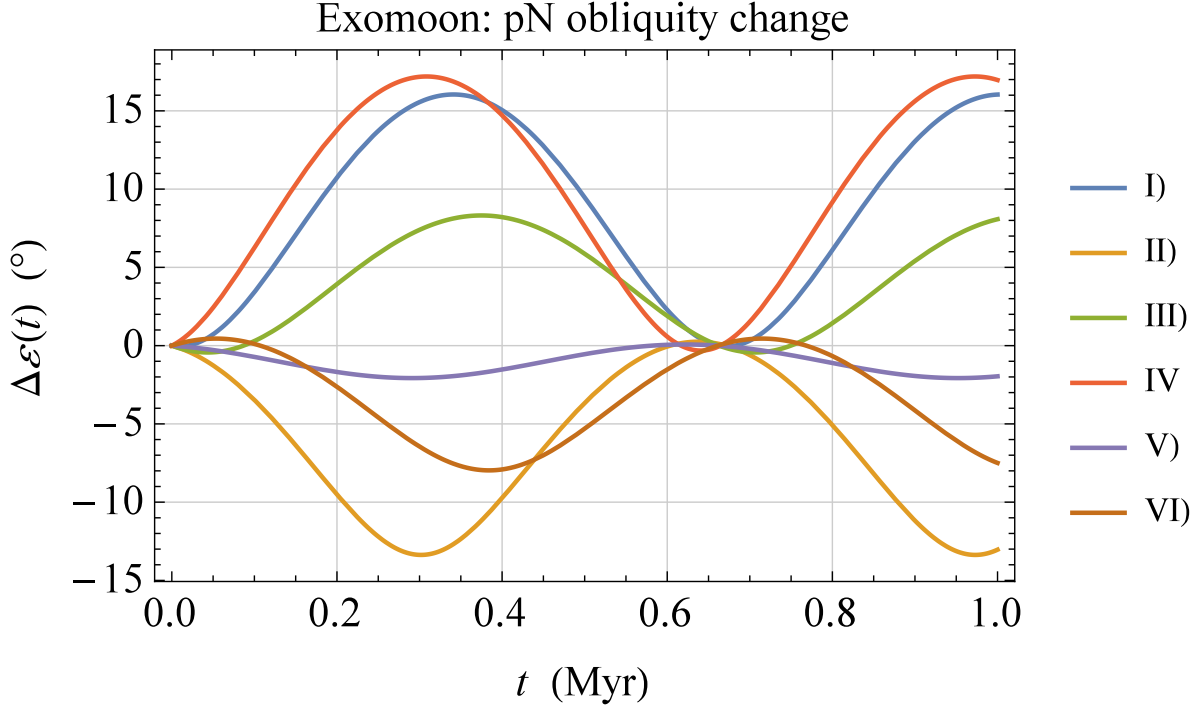


Fig. 1.— Numerically produced time series $\Delta\epsilon(t) = \epsilon(t) - \epsilon_0$, in $^\circ$, of the general relativistic pN variation of the obliquity ϵ to the ecliptic plane of a putative exomoon orbiting a gaseous giant planet with the same physical properties of Jupiter. They were obtained by simultaneously integrating the orbit-averaged Equations (12)-(13) and Equations (25)-(26) for the rates of change of ϵ , α , Ω , I over 1 Myr. The initial conditions, corresponding to a close alignment of $\hat{\mathbf{h}}$, $\hat{\mathbf{j}}$, $\hat{\mathbf{s}}$, are listed in Table 1, which summarizes the main features of the signatures as well.

Table 2 and Figure 2 deal with the case in which the three angular momenta initially share almost the same azimuthal plane, being tilted differently to the ecliptic. It can be noted that $\epsilon_{\max} - \epsilon_{\min}$ ranges from 10° to 150° .

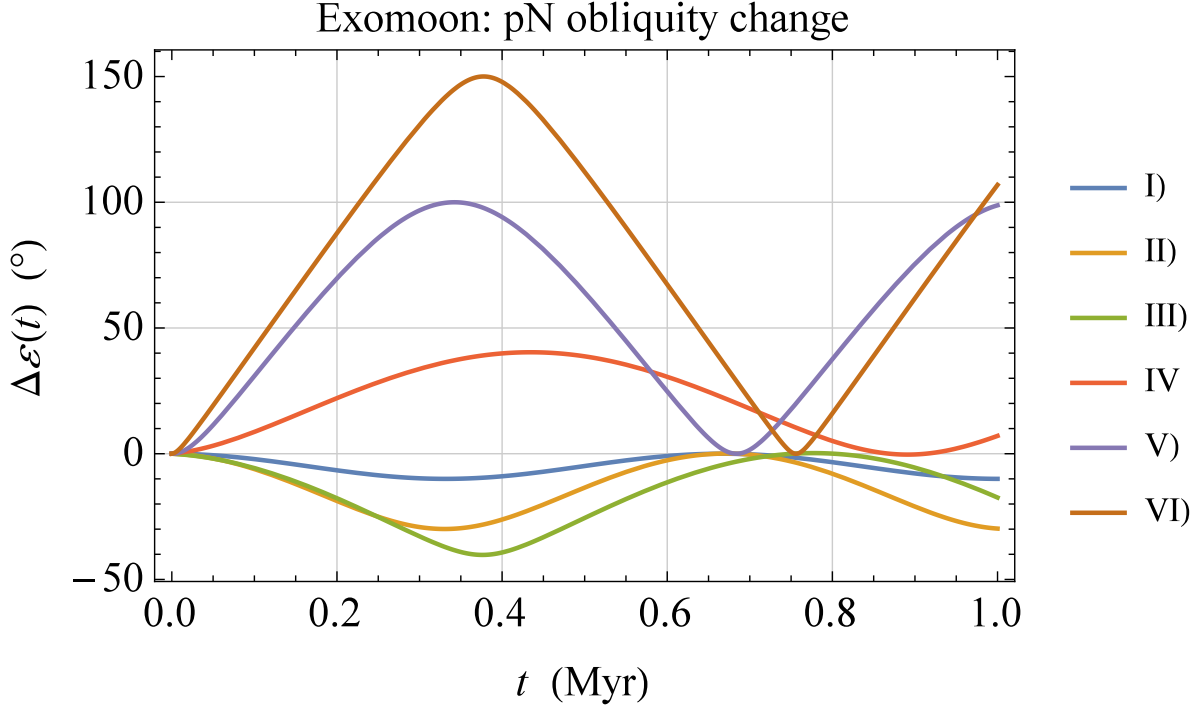


Fig. 2.— Numerically produced time series $\Delta\varepsilon(t) = \varepsilon(t) - \varepsilon_0$, in $^\circ$, of the general relativistic pN variation of the obliquity ε to the ecliptic plane of a putative exomoon orbiting a gaseous giant planet with the same physical properties of Jupiter. They were obtained by simultaneously integrating the orbit-averaged Equations (12)-(13) and Equations (25)-(26) for the rates of change of ε , α , Ω , I over 1 Myr. The initial conditions, corresponding to $\hat{\mathbf{h}}$, $\hat{\mathbf{J}}$, $\hat{\mathbf{S}}$ lying almost in the same azimuthal plane but tilted differently from each other, are listed in Table 2, which summarizes the main features of the signatures as well.

Table 2: Initial conditions used in Figure 2. Each row corresponds to the plotted times series with the same roman numeral in the legend of Figure 2. Recall that the azimuthal angle of $\hat{\mathbf{h}}$ is $\Xi = \Omega - 90^\circ$. T is the characteristic timescale, and $\varepsilon_{\max} - \varepsilon_{\min}$ is the full range of variation of the exomoon’s obliquity to the ecliptic.

	a (R)	e	I_0 ($^\circ$)	Ω_0 ($^\circ$)	η ($^\circ$)	φ ($^\circ$)	ε_0 ($^\circ$)	α_0 ($^\circ$)	T (Myr)	$\varepsilon_{\max} - \varepsilon_{\min}$ ($^\circ$)
I)	5	0.0	15	233	5	147	80	149	0.7	10
II)	5	0.0	30	243	15	146	65	151	0.7	30
III)	5	0.0	65	248	30	148	50	153	0.7	40
IV)	5	0.0	5	242	50	156	30	150	0.7	40
V)	5	0.0	80	240	65	153	15	154	0.7	100
VI)	5	0.0	50	238	80	152	5	147	0.7	150

Table 3 and Figure 3 refer to $\hat{\mathbf{h}}$, $\hat{\mathbf{j}}$, $\hat{\mathbf{s}}$ sharing almost the same tilt to the ecliptic and displaced in different azimuthal planes. In this case, the range of values is narrower than in Figures 1 to 2, amounting to $36^\circ \leq \varepsilon_{\max} - \varepsilon_{\min} \leq 54^\circ$. Nonetheless, it still remains likely significative for the exomoon’s habitability.

Table 3: Initial conditions used in Figure 3. Each row corresponds to the plotted times series with the same roman numeral in the legend of Figure 3. Recall that the azimuthal angle of $\hat{\mathbf{h}}$ is $\Xi = \Omega - 90^\circ$. T is the characteristic timescale, and $\varepsilon_{\max} - \varepsilon_{\min}$ is the full range of variation of the exomoon’s obliquity to the ecliptic.

	a (R)	e	I_0 ($^\circ$)	Ω_0 ($^\circ$)	η ($^\circ$)	φ ($^\circ$)	ε_0 ($^\circ$)	α_0 ($^\circ$)	T (Myr)	$\varepsilon_{\max} - \varepsilon_{\min}$ ($^\circ$)
I)	5	0.0	25 $^\circ$.44	90	29 $^\circ$.44	290	21 $^\circ$.44	250	0.7	37
II)	5	0.0	28 $^\circ$.44	130	18 $^\circ$.44	250	25	290	0.7	36
III)	5	0.0	22 $^\circ$.44	170	24 $^\circ$.44	210	20.50	130	0.7	48
IV)	5	0.0	21 $^\circ$.7	210	27 $^\circ$.44	170	19	90	0.7	54
V)	5	0.0	20 $^\circ$.44	250	22 $^\circ$.44	130	23 $^\circ$.44	210	0.7	44
VI)	5	0.0	19 $^\circ$.44	290	20 $^\circ$.44	90	24 $^\circ$.20	170	0.7	40

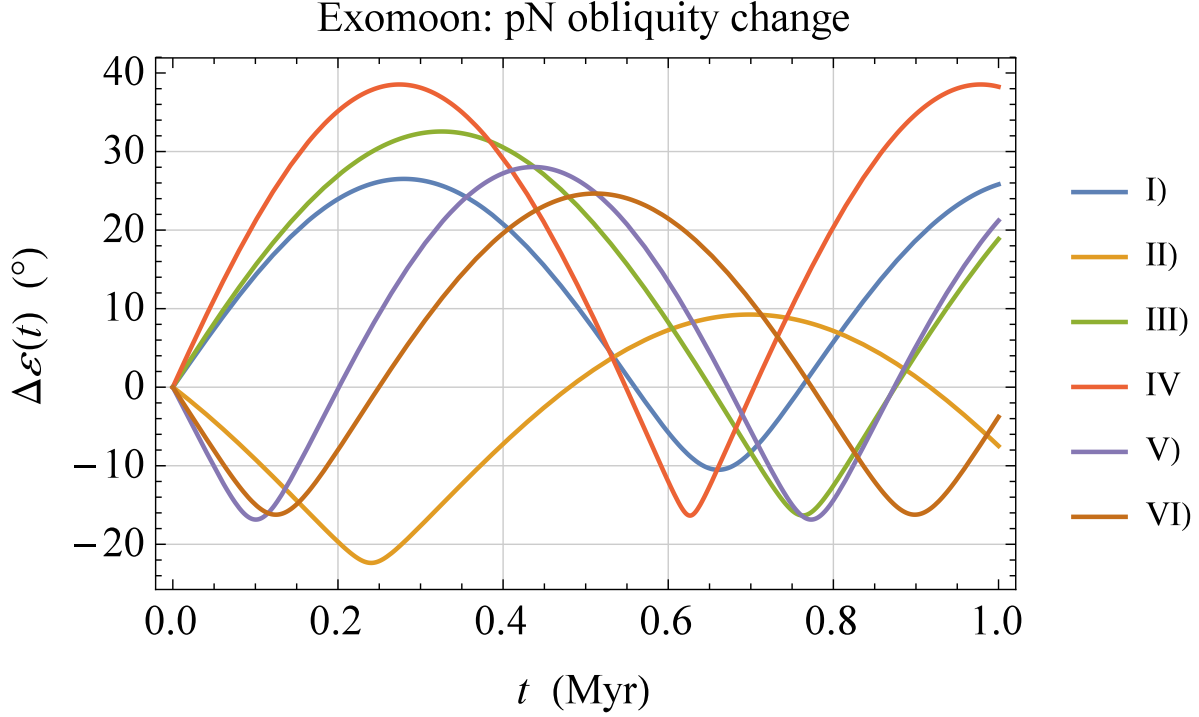


Fig. 3.— Numerically produced time series $\Delta\varepsilon(t) = \varepsilon(t) - \varepsilon_0$, in $^\circ$, of the general relativistic pN variation of the obliquity ε to the ecliptic plane of a putative exomoon orbiting a gaseous giant planet with the same physical properties of Jupiter. They were obtained by simultaneously integrating the orbit-averaged Equations (12)-(13) and Equations (25)-(26) for the rates of change of ε , α , Ω , I over 1 Myr. The initial conditions, corresponding to $\hat{\mathbf{h}}$, $\hat{\mathbf{j}}$, $\hat{\mathbf{s}}$ tilted almost identically to the ecliptic but located in different azimuthal planes, are listed in Table 3, which summarizes the main features of the signatures as well.

The case for an arbitrary mutual orientation of the three angular momenta is displayed by Table 4 and Figure 4. The range of values for the satellite’s obliquity to the ecliptic is $60^\circ - 132^\circ$.

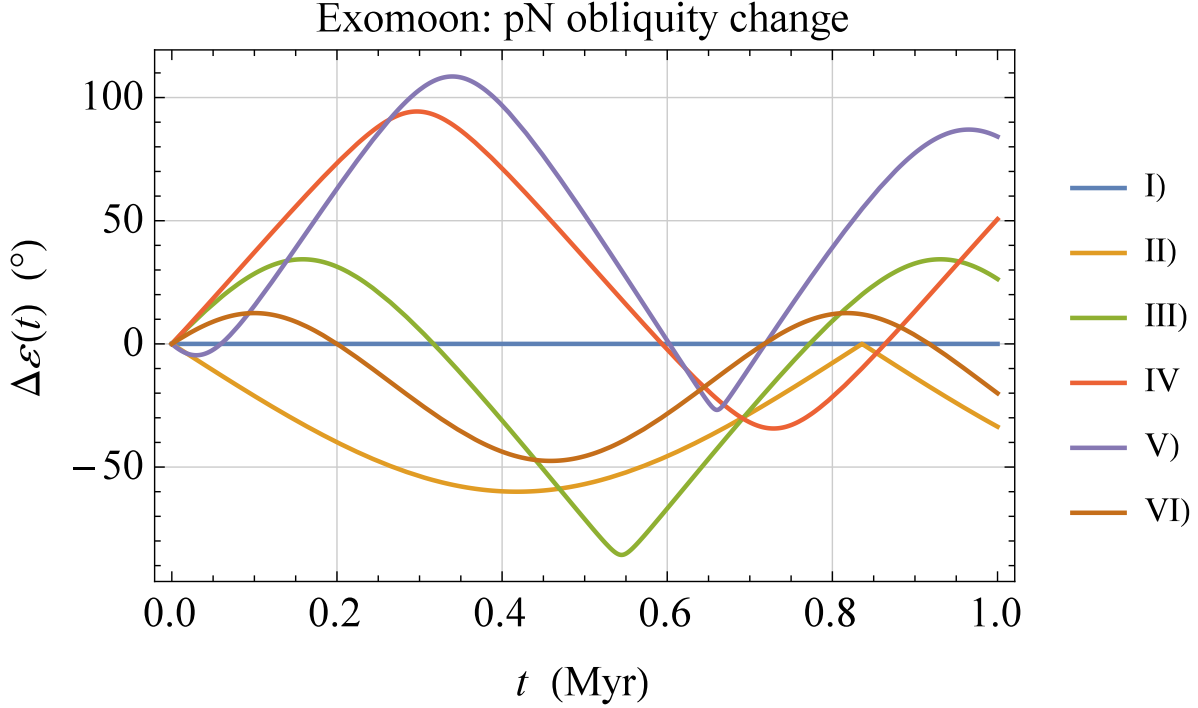


Fig. 4.— Numerically produced time series $\Delta\varepsilon(t) = \varepsilon(t) - \varepsilon_0$, in $^\circ$, of the general relativistic pN variation of the obliquity ε to the ecliptic plane of a putative exomoon orbiting a gaseous giant planet with the same physical properties of Jupiter. They were obtained by simultaneously integrating the orbit-averaged Equations (12)-(13) and Equations (25)-(26) for the rates of change of ε , α , Ω , I over 1 Myr. The initial conditions, corresponding to $\hat{\mathbf{h}}$, $\hat{\mathbf{J}}$, $\hat{\mathbf{S}}$ arbitrarily oriented, are listed in Table 4, which summarizes the main features of the signatures as well.

In Figure 5, obtained for the initial spin-orbit configuration of Table 5, I varied the satellite’s

Table 4: Initial conditions used in Figure 4. Each row corresponds to the plotted times series with the same roman numeral in the legend of Figure 4. Recall that the azimuthal angle of $\hat{\mathbf{h}}$ is $\Xi = \Omega - 90^\circ$. T is the characteristic timescale, and $\varepsilon_{\max} - \varepsilon_{\min}$ is the full range of variation of the exomoon’s obliquity to the ecliptic.

	a (R)	e	I_0 ($^\circ$)	Ω_0 ($^\circ$)	η ($^\circ$)	φ ($^\circ$)	ε_0 ($^\circ$)	α_0 ($^\circ$)	T (Myr)	$\varepsilon_{\max} - \varepsilon_{\min}$ ($^\circ$)
I)	5	0.0	60	0	180	300	150	120	0.7	0.0012
II)	5	0.0	30	60	150	240	180	300	0.7	60
III)	5	0.0	150	120	60	180	90	240	0.7	110
IV)	5	0.0	120	180	90	120	60	0	0.7	120
V)	5	0.0	90	240	120	60	30	180	0.7	132
VI)	5	0.0	180	300	30	0	120	60	0.7	60

planetocentric distance from $5 R$ to $10 R$. As expected from the qualitative analysis of Section 2.2, each time series retains essentially the same maximum range of values $\varepsilon_{\max} - \varepsilon_{\min} \simeq 180^\circ$, while the characteristic timescales of their complicated, non-harmonic temporal patterns, determined by Equation (29), increase with a .

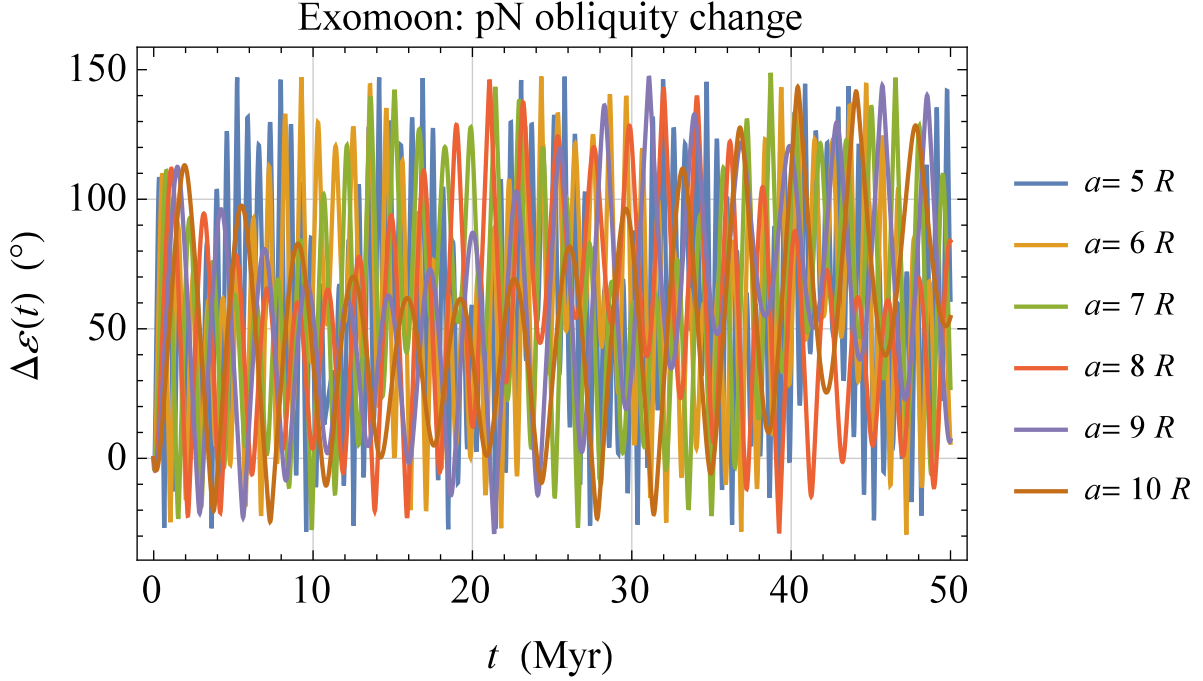


Fig. 5.— Numerically produced time series $\Delta\varepsilon(t) = \varepsilon(t) - \varepsilon_0$, in $^\circ$, of the general relativistic pN variation of the obliquity ε to the ecliptic plane of a putative exomoon orbiting a gaseous giant planet with the same physical properties of Jupiter. They were obtained by simultaneously integrating the orbit-averaged Equations (12)-(13) and Equations (25)-(26) for the rates of change of ε , α , Ω , I over 50 Myr. The initial spin-orbit configuration, common to all the runs, is listed in Table 5.

I checked the validity of Figures 1 to 5, based on the orbit-averaged Equations (12)-(13) and Equations (25)-(26), by numerically integrating the precessional equations of both the satellite’s spin and orbital angular momenta in the vectorial form given by Barker & O’Connell (1975) over the same time spans of the previous runs. In particular, by neglecting all the contributions from

Table 5: Initial spin-orbit configuration used in Figure 5. T is the characteristic timescale, and $\varepsilon_{\max} - \varepsilon_{\min}$ is the full range of variation of the exomoon’s obliquity to the ecliptic.

$I_0 (^\circ)$	$\Omega_0 (^\circ)$	$\eta (^\circ)$	$\varphi (^\circ)$	$\varepsilon_0 (^\circ)$	$\alpha_0 (^\circ)$
90	240	120	60	30	180

the exomoon’s own spin and quadrupole mass moment, I used Equations (7)-(8) for the satellite’s spin, and Equations (27)-(28) for the orbital angular momentum. I adopted the same orbital and physical parameters of the previous integrations along with the same initial conditions. Then, I computed the time series for $\varepsilon(t)$ from the solution for $\hat{S}_z(t)$ as $\varepsilon(t) = \arccos \hat{S}_z(t)$ by obtaining curves indistinguishable from those in Figures 1 to 5 since they differ, at most, by $\approx 0.8^\circ$ over 50 Myr.

The obliquity of the exomoon’s spin axis to the system’s ecliptic plane can, in principle, vary also because of torques of classical origin which, however, depend on the peculiar characteristics of the satellite like its own oblateness of both tidal and centrifugal origin (Ragozzine & Wolf 2009). Instead, the pN effects previously investigated are due only to the spacetime itself deformed by the mass-energy currents of the parent planet.

Variations of the latitudinal insolation received by the exomoon from the host star due to changes in ε so large as those exhibited by Figures 1 to 5 can certainly have a sensible impact on its habitability, representing a novel element which should be taken into account in future studies on the capability of such worlds to sustain life.

4. The case of faster spinning, larger and more massive gaseous giant planets

Until now, I limited myself to the case of a host planet with the same Jovian physical parameters. It is important to look also at other possible gaseous giants with different fundamental characteristics with respect to Jupiter. Recently, for some of them orbiting at a few tens or hundreds of astronomical units from their parent stars, it was possible to determine some key parameters like the mass M , the equatorial radius R and the spinning period P (Bryan et al. 2020). In order to assess the pN effects on the spin axis of possible exomoons of similar planets, I need estimates of their dimensionless quadrupole mass moment J_2 and their spin angular momentum J .

I will consider a gaseous giant planet with the same characteristics of, say, HD 106906b, whose relevant physical parameters are listed in Table 6. According to known formulas retrievable in, e.g., (Murray & Dermott 2000, Chapter 4), (Helled et al. 2011, Eq. (3)), and (Lissauer, Barnes & Chambers 2012, Appendix A), its J_2 and J turn out to be

$$0.5 \lesssim \frac{J_2}{J_2^{\text{Jup}}} \lesssim 2.5, \quad (41)$$

$$27 \lesssim \frac{J}{J_{\text{Jup}}} \lesssim 45. \quad (42)$$

For Jupiter, it is $J_2^{\text{Jup}} = 0.0146966$ (Iess et al. 2018), and $J_{\text{Jup}} = 6.9 \times 10^{38} \text{ J s}$ (Soffel et al. 2003). The ranges of values in Equations (41)-(42) were obtained for $0.1 \lesssim k_2 \lesssim 0.6$ (Ragozzine & Wolf 2009), where k_2 is the planetary Love number (Sterne 1939; Kopal 1959; Ragozzine & Wolf 2009;

Leconte, Lai & Chabrier 2011).

By using the same initial conditions used in Section 3, I numerically integrated Equations (12)-(13) along with Equations (25)-(26) for the planet of Table 6, subsequently confirmed by the integration of the spin and orbit precessional equations in vectorial form by Barker & O’Connell (1975). As expected from the discussion in Section 2.2, the resulting time series are essentially identical to those of Figure 1 to 5, apart from the characteristic timescales which are about one order of magnitude shorter amounting to $\simeq 0.07$ Myr. Indeed, the de Sitter frequency of HD109906b is just 11 times larger than that of Jupiter, being the planetocentric distances the same. Just as an example, in Figure 6, I show the signatures obtained by varying a from $5 R$ to $10 R$ for the same initial spin-orbit configuration of Table 5. Its resemblance with Figure 5 is remarkable, with the exception of the timescale on the horizontal axis which, in this case, is about 10 times shorter.

Table 6: Mass M , equatorial radius R , spinning period P , dimensionless quadrupole mass moment J_2 , and spin angular momentum J of the gaseous giant planet HD109906b. The values of M , R , P were retrieved from Table 3 of Bryan et al. (2020), while J_2 , J were calculated following, e.g., Bourda & Capitaine (2004); Ragozzine & Wolf (2009); Leconte, Lai & Chabrier (2011) by assuming $k_2 = 0.52$ (Ragozzine & Wolf 2009) for the planet’s Love number. Here, M_{Jup} , R_{Jup} , J_2^{Jup} , J_{Jup} are referred to Jupiter.

$M (M_{\text{Jup}})$	$R (R_{\text{Jup}})$	P (hr)	$J_2 (J_2^{\text{Jup}})$	$J (J_{\text{Jup}})$
11	1.56	4	2.2	43.2

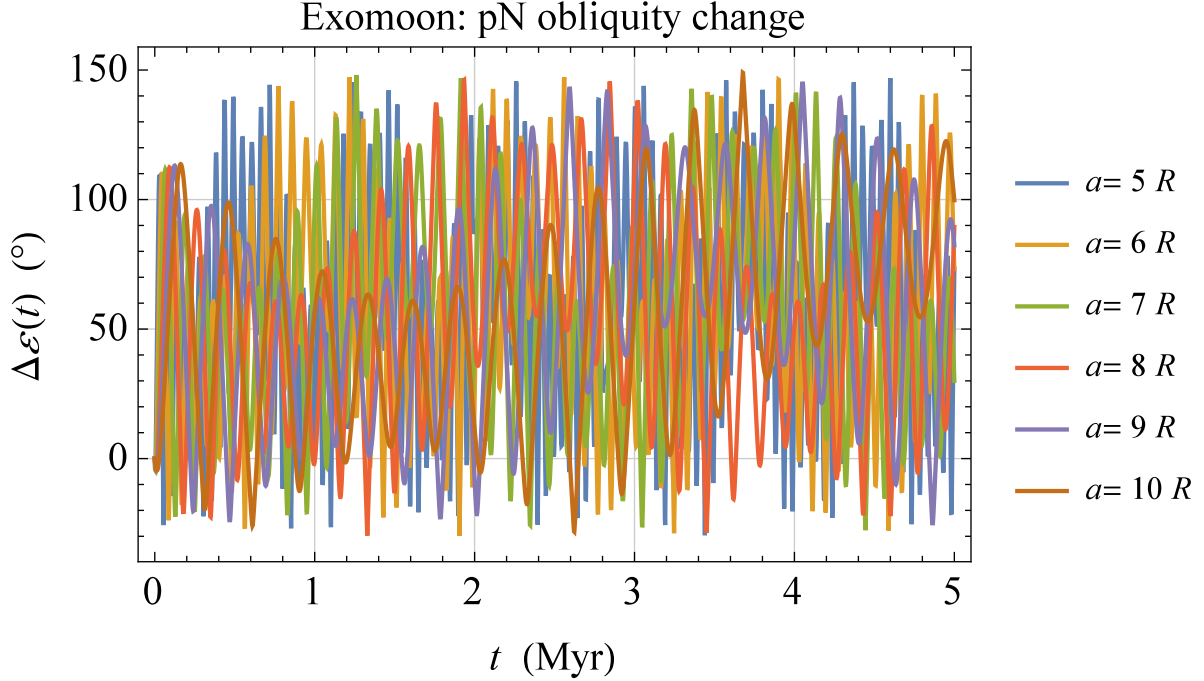


Fig. 6.— Numerically produced time series $\Delta\varepsilon(t) = \varepsilon(t) - \varepsilon_0$, in $^\circ$, of the general relativistic pN variation of the obliquity ε to the ecliptic plane of a putative exomoon orbiting a gaseous giant planet with the same physical properties listed in Table 6. They were obtained by simultaneously integrating the orbit-averaged Equations (12)-(13) and Equations (25)-(26) for the rates of change of ε , α , Ω , I over 50 Myr. The initial spin-orbit configuration, common to all the runs, is listed in Table 5.

5. Summary and Conclusions

I analytically and numerically studied the pN de Sitter and Lense-Thirring precessions of the spin of a spherically symmetric gyroscope freely moving in the deformed stationary spacetime of a massive rotating body for an arbitrary spin-orbit configuration. I applied my results to a putative exomoon orbiting different Jupiter-like gaseous giant planets, assumed to be at 1 au from a Sun-type main sequence star. In particular, I looked at the long-term pN variations $\Delta\varepsilon$ of the satellite’s obliquity ε with respect to its initial value ε_0 . Indeed, the axial tilt is a key parameter in constraining the capability of hosting and sustaining life over long time spans since it controls the insolation received directly from the star at a given body’s latitude. Thus, fast and large temporal changes of ε , like those I found, may likely impact exomoons’ habitability. Its detailed investigation from a climatological and planetological perspective is, however, outside the scopes of the present study.

First, I analytically derived orbit-averaged equations for the pN rates of change of the satellite’s spin obliquity ε and azimuthal angle α along with the equations for the precessions of the orbital inclination I and longitude of ascending node Ω driven by both the classical quadrupole J_2 and the pN Lense-Thirring spin component of the planetary gravitational field; the latter ones enter only indirectly $d\varepsilon/dt$. By neglecting the satellite’s own oblateness, its spin obliquity rate is purely post-Newtonian and, for the considered scenario, mainly gravitoelectric, being the gravitomagnetic Lense-Thirring component 2-3 orders of magnitude smaller. Moreover, the orbital precessions of I and Ω are dominated by the planet’s oblateness by 7 orders of magnitude with respect to the Lense-Thirring ones. Even with such approximations, an exact analytical solution of the resulting system of equations for ε , α , I , Ω cannot be found for an arbitrary spin-orbit configuration. Nonetheless, some qualitative features of $\varepsilon(t)$ can still be inferred. In general, it represents a non-harmonic signal with complex temporal pattern whose characteristic timescale is determined by the de Sitter frequency. Furthermore, its amplitude is independent of the planet’s physical properties and the exomoon’s planetocentric distance, depending only on the initial spin-orbit configuration.

Subsequently, the equations for ε , α , I , Ω were numerically integrated over 1–50 Myr. I started by varying the spin-orbit configuration by keeping the planetocentric distance from a Jupiter-like planet fixed to $5 R$. I considered four different scenarios. First, I assumed \hat{h} , \hat{J} , \hat{S} almost aligned with each other up to a few degrees: the ideal condition of perfect alignment of the three angular momenta would imply the absence of any spin precessions. I found the resulting ranges of variation $\varepsilon_{\max} - \varepsilon_{\min}$ large enough to be likely significant for habitability, amounting to $\simeq 3^\circ - 17^\circ$. Then, I considered the cases in which \hat{h} , \hat{J} , \hat{S} a) Share almost the same azimuthal plane but are differently tilted to the ecliptic b) Are located in different azimuthal planes with almost the same axial tilts c) Are arbitrarily oriented in space. In all such cases, $\Delta\varepsilon$ experiences relevant variations up to tens and, sometimes, even hundreds degrees. All such integrations, covering 1 Myr, exhibit non-harmonic temporal patterns and a characteristic timescale of about 0.7 Myr. Finally, I made numerical integrations over 50 Myr by varying the exomoon’s planetocentric distance from $5 R$ to $10 R$ for a given spin-orbit configuration. I found that, as expected, all the curves for $\Delta\varepsilon$ retain essentially the same amplitudes, showing increasing characteristic timescales with distance.

I successfully tested my results with another set of runs over the same time spans based on the vectorial form of the spin and orbital precessions retrieved in the literature. The resulting times series agree with the previous ones up to less than a degree over 50 Myr.

I looked also at another parent planet for which the physical parameters of the existing exoplanet HD109906b were adopted. In particular, its mass is 11 times larger than that of Jupiter, and its oblateness J_2 and spin angular momentum J can be up to 2.5 and 45 times larger than the Jovian ones. The temporal patterns and the magnitudes of the resulting time series, calculated with the same sets of initial conditions, are similar to those for a Jupiter-like body, but their characteristic timescale is about the order of magnitude shorter. Indeed, the de Sitter frequency of a HD109906b-type planet is just about 10 times larger than that of Jupiter for the same

planetocentric distances.

As directions for future work, I did not investigate the classical and post-Newtonian variations of the obliquity of the exomoon's spin with respect to the plane of its orbit around the host planet, which may be another relevant factor in the total energy balance because of the irradiation from the planet itself due to both the reflected sunlight and the infrared radiation. A further effect which is likely worth of further investigations is the impact of the tidal torques which, among other things, tend to align the orbital angular momentum of the planetocentric orbit with the planet and satellite's spins in order to see if they are effectively counterbalanced by the relativistic signatures obtained here. Also the consequences of the oblateness of the exomoon on its obliquity, both to the ecliptic and to the planetocentric orbital plane, deserve to be studied, along with N-body perturbations induced by other possible major bodies in the system.

In conclusion, the pN temporal variations of the tilt of the exomoon's spin axis to the plane of the planet-satellite's orbit around a distant Sun-like main sequence star are fast and large enough to have most likely a significant impact on its habitability for a variety of different spin-orbit configurations. It is true also in the widely expected scenario in which the satellite's spin is almost aligned with the planetary one and with the planetocentric orbital angular momentum. To my knowledge, it is the first time that it is shown that general relativity may directly have a macroscopic impact on life in a likely common astronomical scenario. Future climatological and planetological studies on the habitability of exomoons should include also such effects in the overall budget of the dynamical constraints to life sustainability.

Data availability

No new data were generated or analysed in support of this research.

REFERENCES

- Armstrong J. C., Barnes R., Domagal-Goldman S., Breiner J., Quinn T. R., Meadows V. S., 2014, *AsBio*, 14, 277
- Armstrong J. C., Leovy C. B., Quinn T., 2004, *Icar*, 171, 255
- Asada H., Futamase T., 1997, *PThPS*, 128, 123
- Barker B. M., O’Connell R. F., 1975, *PhRvD*, 12, 329
- Barnes J. W., O’Brien D. P., 2002, *ApJ*, 575, 1087
- Blanchet L., 2003, in *Proceedings of the Twelfth Workshop on General relativity and Gravitation in Japan*, Shibata M., Eriguchi Y., Taniguchi K., Nakamura T., Tomita K., eds., The University of Tokyo, Komaba, Tokyo, pp. 8–23
- Bourda G., Capitaine N., 2004, *A&A*, 428, 691
- Breton R. P. et al., 2008, *Sci*, 321, 104
- Brumberg V. A., 1991, *Essential Relativistic Celestial Mechanics*. Adam Hilger, Bristol
- Bryan M. L., Ginzburg S., Chiang E., Morley C., Bowler B. P., Xuan J. W., Knutson H. A., 2020, *ApJ*, 905, 37
- Cabrera J., Schneider J., 2007, *A&A*, 464, 1133
- Damour T., Schafer G., 1988, *NCimB*, 101, 127
- Damour T., Taylor J. H., 1992, *PhRvD*, 45, 1840
- de Sitter W., 1916, *MNRAS*, 77, 155
- Debono I., Smoot G. F., 2016, *Univ*, 2, 23
- Deeg H. J., Belmonte J. A., 2018, *Handbook of Exoplanets*. Springer, Cham
- Dickey J. O. et al., 1994, *Sci*, 265, 482
- Dobos V., Heller R., Turner E. L., 2017, *A&A*, 601, A91
- Domingos R. C., Winter O. C., Yokoyama T., 2006, *MNRAS*, 373, 1227
- Everitt C. W. F. et al., 2011, *PhRvL*, 106, 221101
- Everitt C. W. F. et al., 2015, *CQGra*, 32, 224001
- Fokker A. D., 1920, *KNAB*, 29, 611

- Forgan D., Kipping D., 2013, MNRAS, 432, 2994
- Forgan, D., 2019, IJA, 18, 510
- Fox C., Wiegert P., 2021, MNRAS, 501, 2378
- Helled R., Anderson J. D., Schubert G., Stevenson D. J., 2011, Icar, 216, 440
- Heller R., Barnes R., 2013, AsBio, 13, 18
- Heller R., Leconte J., Barnes R., 2011, A&A, 528, A27
- Heller R. et al., 2014, AsBio, 14, 798
- Heller, R., 2012, A&A, 545, L8
- Hill M. L., Kane S. R., Seperuelo Duarte E., Kopparapu R. K., Gelino D. M., Wittenmyer R. A., 2018, ApJ, 860, 67
- Hinkel N. R., Kane S. R., 2013, ApJ, 774, 27
- Hofmann F., Müller J., 2018, CQGra, 35, 035015
- Iess L. et al., 2018, Natur, 555, 220
- Iorio L., 2017, EPJC, 77, 439
- Irwin L. N., Schulze-Makuch D., 2020, Univ, 6, 130
- Kaltenegger L., 2010, ApJ, 712, L125
- Kaltenegger L., 2017, ARA&A, 55, 433
- Kerr R. A., 1987, Sci, 235, 973
- Kilic C., Raible C. C., Stocker T. F., 2017, ApJ, 844, 147
- Kipping D. M., 2009a, MNRAS, 392, 181
- Kipping D. M., 2009b, MNRAS, 396, 1797
- Kipping D. M., Bakos G. Á., Buchhave L., Nesvorný D., Schmitt A., 2012, ApJ, 750, 115
- Kipping D. M., Forgan D., Hartman J., Nesvorný D., Bakos G. Á., Schmitt A., Buchhave L., 2013a, ApJ, 777, 134
- Kipping D. M., Fossey S. J., Campanella G., 2009, MNRAS, 400, 398

- Kipping D. M., Hartman J., Buchhave L. A., Schmitt A. R., Bakos G. Á., Nesvorný D., 2013b, *ApJ*, 770, 101
- Kopal Z., 1959, *Close binary systems*. Chapman & Hall, London
- Kramer M., 2012, in *The Twelfth Marcel Grossmann Meeting. Proceedings of the MG12 Meeting on General Relativity*, Damour T., Jantzen R., Ruffini R., eds., World Scientific, Singapore, pp. 241–260
- Laskar J., Joutel F., Robutel P., 1993, *Natur*, 361, 615
- Laskar J., Robutel P., Joutel F., et al., 2004, *A&A*, 428, 261
- Leconte J., Lai D., Chabrier G., 2011, *A&A*, 528, A41
- Lingam M., Loeb A., 2020, *IJA*, 19, 210
- Linsenmeier M., Pascale S., Lucarini V., 2015, *P&SS*, 105, 43
- Lissauer J. J., 2012, *NewAR*, 56, 1
- Lissauer J. J., Barnes J. W., Chambers J. E., 2012, *Icar*, 217, 77
- Martínez-Rodríguez H., Caballero J. A., Cifuentes C., Piro A. L., Barnes R., 2019, *ApJ*, 887, 261
- Mashhoon B., 2001, in *Reference Frames and Gravitomagnetism*, Pascual-Sánchez J. F., Floría L., San Miguel A., Vicente F., eds., World Scientific, Singapore, pp. 121–132
- Milankovitch M., 1941, *Kanon der Erdbestrahlung und seine Anwendung auf das Eiszeitenproblem*. Belgrad Königliche Serbische Akademie
- Misner C. W., Thorne K. S., Wheeler J. A., 2017, *Gravitation*. Princeton University Press, Princeton
- Mitrovica J. X., Forte A. M., 1995, *GeoJI*, 121, 21
- Murray C. D., Dermott S. F., 2000, *Solar System Dynamics*. Cambridge: Cambridge Univ. Press
- Ohanian H., Ruffini R., 2013, *Gravitation and Spacetime*. Third Edition. Cambridge University Press, Cambridge
- Pais M. A., Le Mouél J. L., Lambeck K., Poirier J. P., 1999, *E&PSL*, 174, 155
- Perryman M., 2018, *The Exoplanet Handbook*. Second edition. Cambridge Univ. Press, Cambridge
- Poisson E., Will C. M., 2014, *Gravity*. Cambridge: Cambridge Univ. Press

- Porter S. B., Grundy W. M., 2011, *ApJ*, 736, L14
- Pugh G., 1959, Proposal for a Satellite Test of the Coriolis Prediction of General Relativity. Research Memorandum 11, Weapons Systems Evaluation Group, The Pentagon, Washington D.C.
- Quarles B., Barnes J. W., Lissauer J. J., Chambers J., 2019, *AsBio*, 20, 73
- Quarles B., Li G., Lissauer J. J., 2019, *ApJ*, 886, 56
- Ragozzine D., Wolf A. S., 2009, *ApJ*, 698, 1778
- Rindler W., 2001, *Relativity: special, general, and cosmological*. Oxford University Press, Oxford, UK
- Rodenbeck K., Heller R., Gizon L., 2020, *A&A*, 638, A43
- Sartoretti P., Schneider J., 1999, *A&AS*, 134, 553
- Sasaki T., Stewart G. R., Ida S., 2010, *ApJ*, 714, 1052
- Schiff L., 1960, *PhRvL*, 4, 215
- Schneider J., Lainey V., Cabrera J., 2015, *IJAsB*, 14, 191
- Schouten W. J. A., 1918, *KNAB*, 27, 214
- Schulze-Makuch D., Bains W., 2018, *NatAs*, 2, 432
- Schwieterman E. W. et al., 2018, *AsBio*, 18, 663
- Seager S., 2011, *Exoplanets*. University of Arizona Press, Tucson
- Shan Y., Li G., 2018, *AJ*, 155, 237
- Soffel M. et al., 2003, *AJ*, 126, 2687
- Soffel M. H., Han W.-B., 2019, *Applied General Relativity*, Astronomy and Astrophysics Library. Springer Nature Switzerland, Cham
- Sterne T. E., 1939, *MNRAS*, 99, 451
- Teachey A., Kipping D. M., 2018, *SciA*, 4, eaav1784
- Teachey A., Kipping D. M., Schmitt A. R., 2018, *AJ*, 155, 36
- Thorne K. S., MacDonald D. A., Price R. H., eds., 1986, *Black Holes: The Membrane Paradigm*. Yale University Press, Yale

- Tjoa J. N. K. Y., Mueller M., van der Tak F. F. S., 2020, *A&A*, 636, A50
- Trifonov T. et al., 2020, *A&A*, 638, A16
- Will C. M., 2008, *ApJL*, 674, L25
- Will C. M., 2018, *Theory and Experiment in Gravitational Physics*. Second edition. Cambridge University Press, Cambridge
- Williams D. M., Kasting J. F., 1997, *Icar*, 129, 254
- Williams D. M., Kasting J. F., Wade R. A., 1997, *Natur*, 385, 234
- Williams J. G., Folkner W. M., 2009, in *IAU Symposium #261*, American Astronomical Society, Vol. 261, p. 882
- Williams J. G., Newhall X. X., Dickey J. O., 1996, *PhRvD*, 53, 6730
- Zollinger R. R., Armstrong J. C., Heller R., 2017, *MNRAS*, 472, 8